Efficient reflection via four-wave mixing in a Doppler-free electromagnetically-induced-transparency gas system

Hai-Tao Zhou,[1] Da-Wei Wang,[2,*] Dan Wang,[1] Jun-Xiang Zhang,[1,*] and Shi-Yao Zhu[1,2,3,4]

[1]*The State Key Laboratory of Quantum Optics and Quantum Optics Devices, Institute of Opto-Electronics, Shanxi University, Taiyuan 030006, China*

[2]*Department of Physics, Centre of Optics Sciences, The Chinese University of Hong Kong, Hong Kong, China*

[3]*Beijing Computational Science Research Center, Beijing 100084, China*

[4]*Department of Physics, Hong Kong Baptist University, Hong Kong, China*

(Received 5 August 2011; published 17 November 2011)

We experimentally demonstrate the high-efficiency reflection of a probe field in Λ-type three-level atoms of cesium vapor driven by two counterpropagating coupling fields. More than 60% of reflection efficiency is observed at the phase-matching angle. The underlying mechanism theoretically is investigated as the four-wave mixing is enhanced by the electromagnetically-induced transparency. Both of the two Doppler-free two-photon resonances (one for the probe and co-propagating fields, the other for the reflected and the counterpropagation fields) play an important role in satisfying the phase matching in the reflection direction. The phase compensation due to the anomalous dispersion and the decrease of effective absorption length in the atomic system allow the efficient reflection to be observed in a wide range of incident angles of the probe field and detunings of the coupling field.

DOI: 10.1103/PhysRevA.84.053835 PACS number(s): 42.50.Gy, 32.80.Qk

I. INTRODUCTION

Four-wave mixing (FWM) is a well-known nonlinear optical effect that generates light with different frequencies and different quantum properties, such as squeezed and entangled fields [1]. The FWM can be enhanced in an electromagnetically-induced transparency (EIT) medium [2,3]. Experimental and theoretical studies reveal that the atomic coherence of the EIT plays an important role in the nonlinear wave-mixing process [4–8]. The EIT-based nonlinear schemes can be driven by traveling wave beams [4–8] and can be driven by a standing wave (SW) due to two counterpropagating coupling fields [9]. The large nonlinearity was obtained in an atomic system driven by two counterpropagating coupling fields [10,11], which form a SW when the two counterpropagating coupling fields have the same frequency. Thus, in this case, the EIT-based nonlinearity can be viewed as a nonlinear grating formed by spatially modulating the strong coupling beam by using a SW [12,13]. This effect, called electromagnetically-induced grating, has a potential use in all optical switching [14], manipulation of light propagation to create a tunable photonic band gap [15,16], and creation of a stationary light pulse (SLP) [13,17].

Although the two counterpropagating fields in crystals [18], as well as in cold atoms [11], are viewed to form the grating, an experimental study on bichromatic SLP in cold atoms shows that the FWM process [17] is not due to the Bragg grating because the Bragg grating could not be established with the bichromatic coupling fields. It was also noted that, when two counterpropagating coupling fields with the same frequency interact with moving atoms, the moving atoms see bichromatic fields rather than a monochromatic SW because of the opposite Doppler shifts of the two coupling fields. The study shows that an atom driven by bichromatic fields has more complicated spectral lines [19] than that of an atom coupled with a monochromatic field [20]. The two counterpropagating fields in the EIT scheme result in a narrow absorption in hot atoms [14] but a transparency in cold atoms [15,21] or a reduced transparency in hot vapor with a buffer gas [13]. The theoretical study of a three-level system coupled with the counterpropagating bichromatic fields shows that the grating could hardly be created due to the frequency difference between the two fields [22]. These results indicate that there exist somewhat different physical processes in the medium of hot atoms and in the medium of cold atoms under the interaction of two counterpropagating fields. In this paper, we extend our previous paper [23] to further investigate the effect of the reflection from a hot cesium vapor coupled with two equal counterpropagating coupling fields. We use a different diagram of an atomic system, in which the phase-matching condition for FWM can be satisfied at the incident angle $\theta = 0.42^\circ$ between coupling and probe beams. This system is used to obtain an efficient FWM process so that as high as a 60% reflection efficiency is observed. More importantly, by using the phase-matched system, the dependence of the reflection on the incident angle and detuning of the coupling field is measured; the theoretical analysis shows that the competition among the angle defection from the phase-matching angle, the phase compensation due to anomalous dispersion, and the absorption of the probe field by the atoms provide an efficient FWM in a wide range of detunings and incident angles of the probe field. We also find that the generation of the reflection field is accompanied by the absorption of both of the weak probe and the counterpropagating coupling field and the amplification of the co-propagating coupling field at the two-photon resonance for the probe and co-propagating coupling fields (also the reflected and counterpropagating coupling fields). Note, in the case of hot atoms, the probe and the counterpropagating coupling fields (also the reflected and co-propagating coupling fields) could not form the two-photon resonance, which is different from that in the

*junxiang@sxu.edu.cn; cuhkwdw@gmail.com

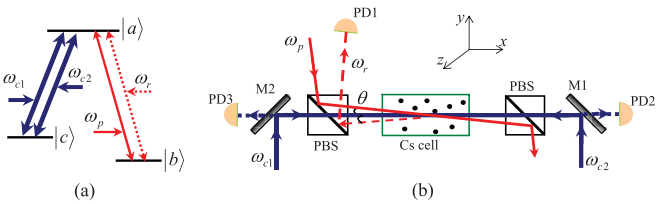

FIG. 1. (Color online) (a) Λ-type three-level scheme. (b) Experimental setup. Polarizing beam splitter (PBS); PD1–3, photodetectors; M1 and M2, mirrors with reflectivity ∼99.9%; and ω_p, ω_r, ω_{c1}, and ω_{c2}, the frequency of the probe, reflected, and co- and counterpropagating coupling fields.

case of cold atoms. The theoretical calculation, based on the FWM enhanced by the EIT, supports the experimental observations.

II. THE MEASUREMENT OF THE REFLECTION SPECTRUM

The experimental setup for studying the reflection of an incident field in the ^{133}Cs gas cell is shown in Fig. 1, similar to that of our previous paper [23] with the two coupling transitions switched. Two strong counterpropagating coupling fields $\mathbf{E}_c(\mathbf{r},t) = (\hat{y}/2)\{E_1\exp[-i(\omega_c t - \mathbf{k}_c\cdot\mathbf{r})] + E_2\exp[-i(\omega_c t + \mathbf{k}_c\cdot\mathbf{r})]\} + \text{c.c.}$ with frequency ω_c couple the transition from $|a\rangle$ $(6^2P_{1/2}, F' = 4)$ to $|c\rangle$ $(6^2S_{1/2}, F = 4)$ with transition frequency ω_{ac}. A co-propagating weak probe field $\mathbf{E}_p(\mathbf{r},t) = (\hat{z}/2)E_p\exp[-i(\omega_p t - \mathbf{k}_p\cdot\mathbf{r})] + \text{c.c.}$ with frequency ω_p couples the transition $|a\rangle$ $(6^2P_{1/2}, F' = 4)$ to $|b\rangle$ $(6^2S_{1/2}, F = 3)$ with transition frequency ω_{ab} as shown in Fig. 1(a). The natural decay of the upper state $|a\rangle$ is $2\pi \times 4.6$ MHz. E_1 and E_2 are the field amplitudes of co- and counterpropagating coupling fields, respectively, in the y direction, and E_p is the amplitude of the probe field in the z direction. The direction of the wave vector of the co-propagating fields $\mathbf{k}_c$ is defined as the $\hat{x}$ axis. The wave vector of the probe field $\mathbf{k}_p$ has an angle θ to the $\hat{x}$ axis. The arrangement of the experiment is shown in Fig. 1(b). An extended diode-laser beam is divided into two beams as the coupling fields, which propagate from opposite directions through a 7.5-cm-long ^{133}Cs vapor cell with anti-reflection-coated end windows (the loss of the far-off resonant light through the cell is 4%). The vapor cell is mounted inside a three-layer μ-metal magnetic shield in order to reduce stray magnetic fields, and the residual magnetic field inside the shield is measured to be about 10 mG. A second extended cavity diode-laser beam (probe) with orthogonal polarization intersects the co-propagating coupling beam at a small angle θ. In our experiment, the power of each coupling field is about 20 mW, and the probe field is 300 μW. The e^{-2} full widths of the probe and coupling fields are 0.59 and 0.64 mm, respectively.

When the frequency of the coupling fields is locked at resonance to the transition between $|a\rangle$ and $|c\rangle$, and meanwhile, the probe field, whose frequency is scanned across the transition $|a\rangle \leftrightarrow |b\rangle$, is applied, a signal with the same frequency as that of the probe field $(\omega_r = \omega_p)$ is generated in the reflection direction [red dashed line in Fig. 1(b)] of the probe field. The reflection efficiency R [the ratio of reflected signal power to input probe power in Eq. ([9]) in the following section] versus the probe detuning $\Delta_p = \omega_p - \omega_{ab}$ for different angles θ is plotted in Fig. 2, and the maximum reflection happens at $\theta \simeq 0.42°$, which satisfies the phase-matching condition $\mathbf{k}_p - 2\mathbf{k}_c - \mathbf{k}_r = 0$, where k_r is the wave vector of the reflected signal [the scalar phase matching $\Delta k_x = 2(\omega_p\cos\theta - \omega_c)/c = 0$ is satisfied for $\theta = 0.42°$ and $\omega_p - \omega_c = 9.2$ GHz in our experiment]. The power of the reflected signal can reach more than 55% of the input probe power. There is a dip at $\omega_p = \omega_{ab}$, which is due to the high absorption of hot atoms driven by two counterpropagating coupling fields [23]. At other angles $\theta \neq 0.42°$, the phase-matching condition cannot be satisfied; the reflection peak does not appear at resonance with lower efficiency. At the angle $\theta < 0.42°$ (or $\theta > 0.42°$), the angle-induced phase mismatch is positive (or negative); the peak appears at $\omega_p > \omega_{ab}$ (or $\omega_p < \omega_{ab}$). The angle dependence of positions of the reflection peak is theoretically analyzed in the next section.

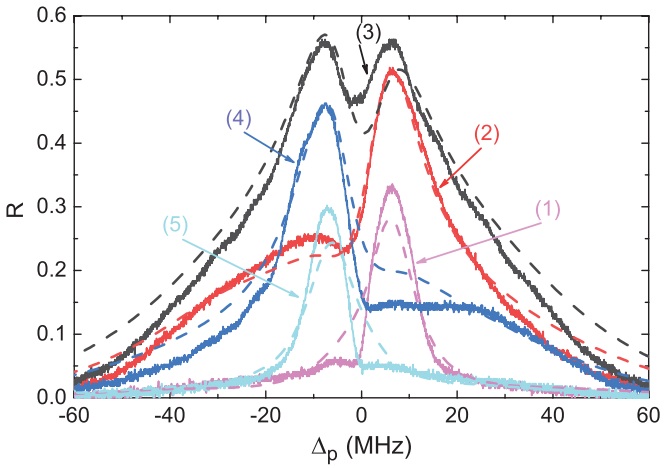

FIG. 2. (Color online) The reflection signal versus probe detuning for different incident angles θ: (1) $\theta = 0.28°$ (light magenta lines), (2) $\theta = 0.38°$ (red lines), (3) $\theta = 0.42°$ (black lines), (4) $\theta = 0.47°$ (blue lines), and (5) $\theta = 0.52°$ (light cyan lines). The solid lines are the experimental data, and the dashed lines are the theoretical calculations, respectively. The probe power is $P_p = 300$ μW, each of the coupling powers is $P_c = 20$ mW, and the set temperature of vapor cell is $T = 35\,°$C. The theoretical parameters are $\Omega_p = 21.5$, $\Omega_c = 162$ MHz, $N = 0.9 \times 10^{10}$ cm^{-3}, $\Gamma = 2\pi \times 4.6$ MHz, and $d_{\text{eff}} = 1.26$ cm.

In Fig. 3, the dependence of the reflection efficiency on angle θ is plotted for two different temperatures of the vapor cell (corresponding to the different densities of the atoms). We can see that the efficiency reaches the maximum at $\theta \simeq 0.42°$, and there is no significant difference in the efficiency at $\theta \simeq 0.42°$ for both of the two temperatures. However, the efficiency at $T = 31\,°$C decreases quicker than that at $T = 35\,°$C with increasing or decreasing θ, and this effect cannot be interpreted solely by the phase mismatching. To explain these observed effects, the compensation of angular phase mismatch by anomalous dispersion and the effective length of absorption medium $d_{\text{eff}} = \int_0^L \exp(-\alpha x)\,dx \approx 1/\alpha$ (α is the absorption coefficient) need to be considered (see the following theoretical discussion). The theoretical calculation

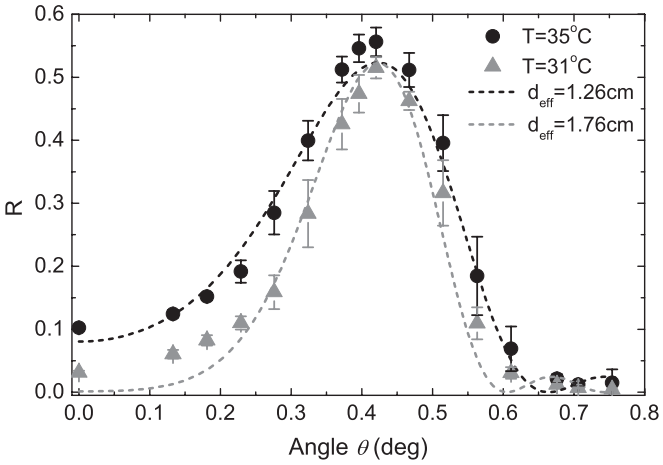

FIG. 3. (Color online) The peak heights of the reflection normalized by incident probe power versus different incident angle θ's. The solid dots are the experimental data, and the dashed lines are the theoretical calculations. The other parameters are the same as that in Fig. 2.

fits the experimental results quite well, see the dashed lines in Figs. 2 and 3.

III. THEORETICAL DISCUSSION

The equations of motion for the density-matrix elements in the three-level system as shown in Fig. 1(a) are

$$\dot{\rho}_{ab} = (-i\omega_{ab} - \gamma_{ab})\rho_{ab} + (i/2)(\Omega_1 e^{-i\omega'_{c1}t} + \Omega_2 e^{-i\omega'_{c2}t})\rho_{cb} + (i/2)\Omega_p e^{-i\omega'_p t}, \quad (1a)$$

$$\dot{\rho}_{cb} = (-i\omega_{cb} - \gamma_{cb})\rho_{cb} + (i/2)(\Omega_1^* e^{i\omega'_{c1}t} + \Omega_2^* e^{i\omega'_{c2}t})\rho_{ab}, \quad (1b)$$

where $\Omega_p = (\mu_{ab}E_p/\hbar), \Omega_{1,2} = (\mu_{ac}E_{1,2}/\hbar)$ are the Rabi frequency of the probe field and co- and counterpropagating coupling fields, μ_{ab}, μ_{ac} are the relevant dipole moments of transitions $|a\rangle \leftrightarrow |b\rangle$ and $|a\rangle \leftrightarrow |c\rangle$, γ_{ab} is the decay rate from excited state $|a\rangle$ to ground state $|b\rangle$, and γ_{cb} is the dephasing rate between two ground states $|b\rangle$ and $|c\rangle$. In Eq. (1), we have performed the approximations that $\rho_{aa} = \rho_{cc} = \rho_{ac} \cong 0, \rho_{bb} = 1$ under the perturbation condition $\Omega_p \ll \Omega_{1,2} \ll (\omega_{ab} - \omega_{ac})$. Consider the atom with velocity v moving along the x direction; it sees the probe with frequency $\omega'_p = \omega_p - k_p v$, where $-k_p v$ is the Doppler shift, and sees the co- and counterpropagating coupling beams with frequencies $\omega'_{c1} = \omega_{c1} - k_c v$ and $\omega'_{c2} = \omega_{c2} + k_c v$, respectively. The frequency difference between the two coupling fields for the moving atoms v is twice the Doppler shift $\omega'_{c2} - \omega'_{c1} = \delta = 2k_c v$, which is about one quarter of the decay rate of the excited state [24] for average velocity.

The solution of Eq. (1) (to first order of E_p and all orders of $E_{1,2}$) can be found in terms of the Fourier amplitudes $\tilde{\rho}_{ij}^{[n]}$,

$$\rho_{ab} = \sum_n \tilde{\rho}_{ab}^{[n]} e^{-\omega'_p t} e^{-in\delta t}, \quad (2a)$$

$$\rho_{cb} = \sum_n \tilde{\rho}_{cb}^{[n]} e^{-i(\omega'_p - \omega'_{c1})} e^{-in\delta t} (n = 0, \pm 1, \ldots). \quad (2b)$$

The solution of $\tilde{\rho}_{ab}^{[n]}$ is determined by the recursion relation,

$$\tilde{\rho}_{ab}^{[n]} = \frac{-i\Omega_p \delta_{n,0} - i\Omega_1 \tilde{\rho}_{cb}^{[n]} - i\Omega_2 \tilde{\rho}_{cb}^{[n-1]}}{i\Delta_p - \gamma_{ab} + in\delta}, \quad (3a)$$

$$\tilde{\rho}_{cb}^{[n]} = \frac{-i\Omega_1^* \tilde{\rho}_{ab}^{[n]} - i\Omega_2^* \tilde{\rho}_{ab}^{[n+1]}}{i(\Delta_p - \Delta_{c1}) - \gamma_{cb} + in\delta}. \quad (3b)$$

The zero- and first-order $\tilde{\rho}_{ab}^{[0]}$ and $\tilde{\rho}_{ab}^{[1]}$, which are related to linear and nonlinear susceptibilities via the polarization relation, can be obtained

$$\tilde{\rho}_{ab}^{[0]} = \frac{-\Omega_p}{P_0 - \frac{\Omega_1\Omega_2^* Z_1}{(\Delta'_p - \Delta'_{c1}) + i\gamma_{cb}} - \frac{\Omega_1^*\Omega_2 X_1}{(\Delta'_p - \Delta'_{c2}) + i\gamma_{cb}}}, \quad (4a)$$

$$\tilde{\rho}_{ab}^{[1]} = \frac{-\Omega_p \Omega_1^* \Omega_2}{P_0 - \frac{\Omega_1\Omega_2^* Z_1}{(\Delta'_p - \Delta'_{c1}) + i\gamma_{cb}} - \frac{\Omega_1^*\Omega_2 X_1}{(\Delta'_p - \Delta'_{c2}) + i\gamma_{cb}}} \frac{U}{1 - \frac{|\Omega_1|^2|\Omega_2|^2 T_1}{1 - \cdots}}, \quad (4b)$$

where $P_n = (\Delta'_p + n\delta + i\gamma_{ab}) - \{|\Omega_1|^2/[(\Delta'_p - \Delta'_{c1}) + n\delta + i\gamma_{cb}] + |\Omega_2|^2/[(\Delta'_p - \Delta'_{c2}) + n\delta + i\gamma_{cb}]\}$, $\Delta'_p = \omega'_p - \omega_{ab}, \Delta'_{c1} = \omega'_{c1} - \omega_{ac}$, $\Delta'_{c2} = \omega'_{c2} - \omega_{ac}$, $U = \{P_1[(\Delta'_p - \Delta'_{c2}) + \delta + i\gamma_{cb}]\}^{-1}, Z_1 = \tilde{\rho}_{ab}^{(1)}/\tilde{\rho}_{ab}^{(0)}$, $X_1 = \Omega_1\Omega_2^* K_1/[1 - |\Omega_1|^2|\Omega_2|^2 L_1/(1 - \cdots)]$, and $T_1 = \{P_1 P_2[(\Delta'_p - \Delta'_{c1}) + \delta + i\gamma_{cb}][(\Delta'_p - \Delta'_{c1}) + 2\delta + i\gamma_{cb}]\}^{-1}$ with $K_1 = \{P_{-1}[(\Delta'_p - \Delta'_{c1}) - \delta + i\gamma_{cb}]\}^{-1}$, $L_1 = K_2\{P_{-1}[(\Delta'_p - \Delta'_{c2}) - \delta + i\gamma_{cb}]\}^{-1}$, and $K_2 = \{P_{-2}[(\Delta'_p - \Delta'_{c1}) - 2\delta + i\gamma_{cb}]\}^{-1}$.

Then, the linear and nonlinear susceptibilities can be obtained from the linear and nonlinear polarizations $P^{(1)}(\omega'_p) = \varepsilon_0\chi^{(1)}E_p(\omega'_p)$ and $P(\omega'_p - \omega'_{c1} + \omega'_{c2}) = 6\varepsilon_0\chi^{(3)}E_p E_1^* E_2$ as [18]

$$\chi^{(1)} = \frac{N|\mu_{ab}|^2}{\varepsilon_0\hbar\Omega_p}\frac{2\sqrt{\ln 2}}{\sqrt{\pi}\Delta\omega_D}\int_{-\infty}^{+\infty}\tilde{\rho}_{ab}^{[0]} \times \exp\left[-\Delta_d^2/(\Delta\omega_D/2\sqrt{\ln 2})^2\right]d\Delta_d, \quad (5a)$$

$$\chi^{(3)} = \frac{N|\mu_{ab}|^2|\mu_{ac}|^2}{6\varepsilon_0\hbar^3\Omega_2\Omega_1^*\Omega_p}\frac{2\sqrt{\ln 2}}{\sqrt{\pi}\Delta\omega_D}\int_{-\infty}^{+\infty}\rho_{ab}^{[1]} \times \exp\left[-\Delta_d^2/(\Delta\omega_D/2\sqrt{\ln 2})^2\right]d\Delta_d, \quad (5b)$$

where ε_0 is the free-space permittivity and N is the atom number density. In Eq. (5), the Doppler effect of the atoms in the vapor cell has been taken into account. The Doppler shift and the full width at half maximum of the absorption profile are $\Delta_d = v\omega_p/c$ and $\Delta\omega_D = 2\omega_p(2\ln 2\, k_B T/mc^2)^{1/2}$, with $(2\,k_B T/mc^2)^{1/2}$ as the most probable speed of the atoms at a given temperature T, m is the atomic mass, and k_B is the Boltzmann constant.

The real and imaginary parts of $\chi^{(1)}$ correspond to the probe's dispersion and absorption. The real part of $\chi^{(3)}$ leads to an efficient FWM. From Eq. (2a), we can deduce that the frequency of the generated field is $\omega_r = \omega_p - (\mathbf{k}_p - \mathbf{k}_r - 2\mathbf{k}_c)\cdot\mathbf{v}$, which depends on the atomic velocity. When the phase-matching condition $\Delta\mathbf{k} = \mathbf{k}_p - \mathbf{k}_r - 2\mathbf{k}_c = 0$ is satisfied, the frequency of the generated field is equal to ω_p, and all the atoms contribute coherently to the generated field. In this case, the direction of the generated field is determined by the phase-matching condition, and it is in the reflection direction of

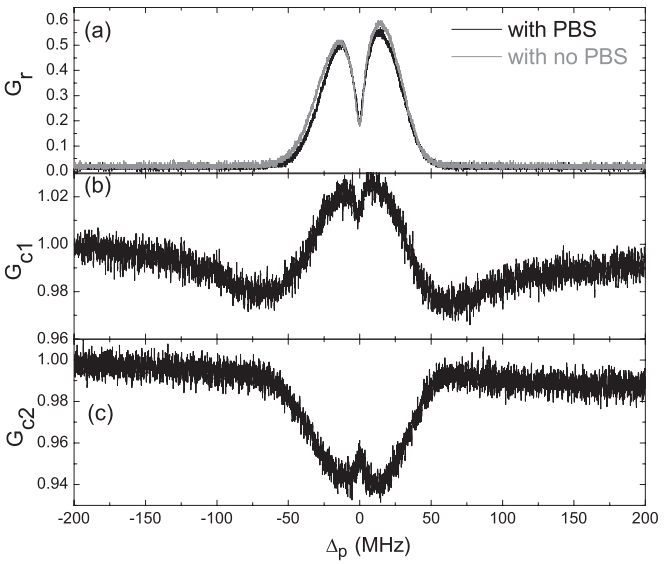

FIG. 4. The gain spectra of the reflected and co- and counterpropagating coupling fields. The experimental parameters are $P_p = 1$, $P_c = 20$ mW, and $T = 35\,^{\circ}$C.

the probe beam. The FWM process determined by the energy conservation and phase-matching condition is as follows: The atom in ground state $|b\rangle$ absorbs one probe photon $\hbar\omega_p'$ and is excited to excited state $|a\rangle$, emits one co-propagating photon $\hbar\omega_{c1}'$ with a transition to $|c\rangle$ (note, a Doppler-free one), then absorbs one counterpropagating photon $\hbar\omega_{c2}'$ back to $|a\rangle$, and finally coherently decays to $|b\rangle$ with the reflection of a FWM photon $\hbar\omega_r = \hbar(\omega_p + \delta)$ (another Doppler-free one). Therefore, the generation of the FWM field is accompanied by the enhancement of the co-propagating coupling field and the attenuations of the probe and counterpropagating fields, as shown in Fig. 4, where G_{c1} and G_{c2} are the measured gains for co- and counterpropagrating coupling fields; they are defined in terms of a power ratio (output power divided by input power). G_r represents the ratio of reflected power to input probe power. In the experiment, in order to exclude the effect from the nonlinear magneto-optical rotation [25–30], we also perform it by removing all polarization sensitivity devices (i.e., PBS) to improve the experimental setup. See Fig. 4(a); the reflection spectrum is detected before a PBS (gray line) or after a PBS (black line). Obviously, as can be seen, except for an intensity loss from the imperfect extinction of the PBS, the shape of the reflected signal has not changed. Similarly, the profile of the co-prorogating and counterpropagating coupling fields are the same as the preceding results. So, we recognize that the dips near the resonant transition of the three curves in Fig. 4 do not result from the optical rotation but rather from the effect of the enhanced absorption of the atomic transition center. The increase in the power of the co-propagating coupling approximately equals the decrease in that of the counterpropagating coupling field. Because of the intensity increasing and decreasing during the propagation of the co-propagating and counterpropagating fields, respectively, the two intensities are never equal in the vapor cell, which makes the formation of a high-visible grating for high-reflection efficiency almost impossible. Moreover, the FWM is enhanced by the ground-state coherence [23], see Eq. (3b) with $n = 0$, which is created by the co-propagrating probe and the copropagating coupling fields at the Doppler-free two-photon resonance. For higher order $\tilde{\rho}_{ab}^{[n]}$ ($n > 1$), the contribution of $\tilde{\rho}_{ab}^{[n]}$ (with $n \neq 0,1$) is small due to the large phase mismatching $\Delta\mathbf{k} = \mathbf{k}_p - \mathbf{k}_r - 2n\mathbf{k}_c$ so that the nth-order generated signal is too small to be considered.

In order to estimate the reflection efficiency, the co- and countermoving propagating equation for the slowly varying components of the probe and generated signal fields [$E_p(x)$ and $E_r(x)$, respectively] are used to achieve this result. We start from the nonlinear coupled wave equations [31],

$$\frac{\partial}{\partial x}E_p(x) = -\alpha E_p(x) + \kappa e^{-i\Delta k_x x}E_r(x), \tag{6a}$$

$$-\frac{\partial}{\partial x}E_r(x) = -\alpha E_r(x) + \kappa e^{i\Delta k_x x}E_p(x), \tag{6b}$$

where $\alpha = (\omega_p/c)\mathrm{Im}\chi^{(1)}/2$ is the attenuation of the field due to the absorption of the medium and $\kappa = i(\omega_p/c)\chi^{(3)}/2$ is related to the nonlinear susceptibility induced by $\tilde{\rho}_{ab}^{[1]}$ in Eq. (5). The general solutions of Eqs. (6) are

$$E_p = C_1^+ e^{\lambda_1^+ x} + C_1^- e^{\lambda_1^- x}, \tag{7a}$$

$$E_r = \frac{\lambda_1^+ + \alpha}{\kappa}C_1^+ e^{\lambda_2^+ x} + \frac{\lambda_1^- + \alpha}{\kappa}C_1^- e^{\lambda_2^- x}, \tag{7b}$$

where $\lambda_1^\pm = -i\Delta k_x/2 \pm [(\alpha - i\Delta k_x/2)^2 - \kappa^2]^{1/2}$ and $\lambda_2^\pm = \lambda_1^\pm + i\Delta k_x$. Δk_x is the scalar phase mismatch at angle θ,

$$\Delta k_x = \{2(\omega_p\cos\theta - \omega_c) + \mathrm{Re}[\chi^{(1)}]\omega_p\cos\theta\}/c. \tag{8}$$

The coefficient $C_1^\pm$ can be determined by the initial condition, which is $E_p(0) = E_0$ and $E_r(d_x) = 0$ in our experiment. The length of the sample in the x direction is d_x. Then, the reflectivity R and transmission T are given as

$$R = \left|\frac{E_r(0)}{E_p(0)}\right|^2 = \left|\frac{1}{\kappa}\frac{e^{-\lambda_2^+ d_x} - e^{-\lambda_2^- d_x}}{e^{-\lambda_2^+ d_x}(\lambda_1^+ + \alpha)^{-1} - e^{-\lambda_2^- d_x}(\lambda_1^- + \alpha)^{-1}}\right|^2, \tag{9a}$$

$$T = \left|\frac{E_p(d_x)}{E_p(0)}\right|^2 = \left|\frac{e^{(\lambda_1^+ + \lambda_1^-)d_x}(\lambda_1^- - \lambda_1^+)}{(\lambda_1^- + \alpha)e^{\lambda_1^- d_x} - (\lambda_1^+ + \alpha)e^{\lambda_1^+ d_x}}\right|^2. \tag{9b}$$

Using Eq. (9a), we plot the reflection efficiency (dashed line) in Fig. 2. The theoretical calculation is consistent with the experimental data. The minor difference may come from the various loss effects as well as the intensity changes of the coupling fields, which are not included in the theoretical calculation. We would like to emphasize that the role of the phase compensation (the second term in Δk_x, $\mathrm{Re}[\chi^{(1)}]\omega_p\cos\theta/c$) due to the anomalous dispersion [23] occurs around the phase-matching angle of $\theta = 0.42^{\circ}$. For $\theta < 0.42^{\circ}$, the first term in Δk_x, Eq. (8), is larger than 0; the phase-matching condition can be satisfied only if the second term is $\mathrm{Re}[\chi^{(1)}]\omega_p\cos\theta/c < 0$, which happens at $\omega_p > \omega_{bc}$ because of the anomalous dispersion of $\mathrm{Re}[\chi^{(1)}]$ [23] so that the peak appears at $\omega_p > \omega_{bc}$. On the other hand, for

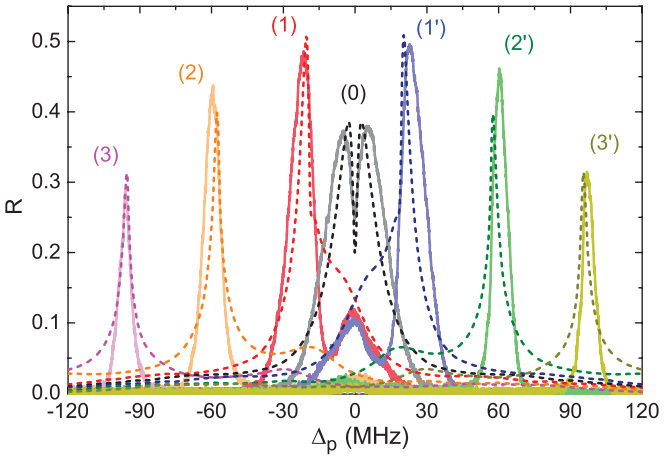

FIG. 5. (Color online) The reflection spectrum versus the detuning of the probe light for different detunings of the coupling field under the condition of phase matching ($\theta = 0.42°$). (0) $\Delta_c = 0$; (1) and (1′) $\Delta_c = -19$ and $+19$ MHz; (2) and (2′) $\Delta_c = -57$ and $+57$ MHz; (3) and (3′) $\Delta_c = -95$ and $+95$ MHz. The experimental parameters are $P_p = 1$, $P_c = 4$ mW, and $T = 35\,°$C. The theoretical parameters are $\Omega_p = 39$, $\Omega_c = 72$ MHz, $N = 0.9 \times 1\ 0^{10}$ cm^{-3}, $\Gamma = 2\pi \times 4.6$ MHz, and $d_{\text{eff}} = 1.85$ cm.

$\theta > 0.42°$, the phase compensation induced by the anomalous dispersion can lead the peak to appear at $\omega_p < \omega_{bc}$.

In the theoretical calculation of the angle dependence of the peak height in Fig. 3, we use Eq. (8) to take the dispersion compensation of the phase mismatch into account, while we use an effective length $d_{\text{eff}} = \int_0^{d_x} e^{-\alpha x} dx \approx 1/\alpha$ to reflect the absorption. Note that d_{eff} decreases with an increase of the absorption, the temperature, and the density of atoms, which is estimated on the order of 1 cm for a 7.5-cm absorption medium. The efficiency of reflection is highly dependent on the phase mismatch and d_{eff} at $\theta \neq 0.42°$ because it is dominated by the exponential terms in Eq. (9). In Fig. 3, d_{eff} is used for a different situation: $d_{\text{eff}} = 1.26$ cm for $T = 35\,°$C and $d_{\text{eff}} = 1.76$ cm for $T = 31°$C. The competition between the absorption and the dispersion compensation determines the efficiency in Fig. 3.

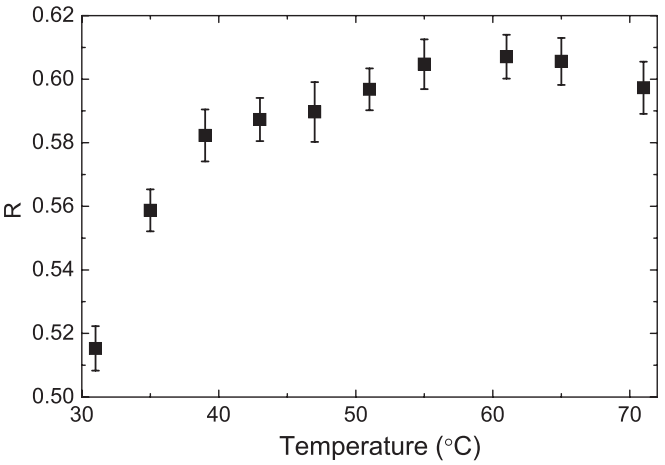

FIG. 6. The efficiency of the reflection peak versus the temperature. The experimental parameters are $P_p = 300$ μW, $P_c = 20$ mW, $\theta = 0.42°$, and $\Delta_c = 0$.

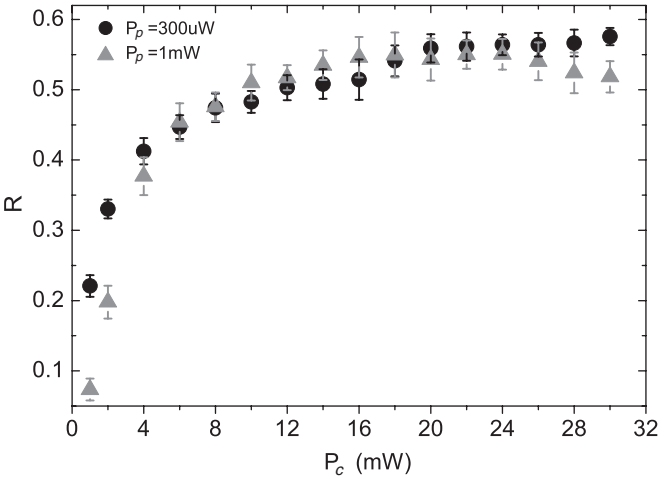

FIG. 7. The efficiency of reflection versus the power of the coupling field with two different powers of the probe: (1) $P_p = 300$ μW (black circle) and (2) $P_p = 1$ mW (gray triangle). The other experimental parameters are $\Delta_c = 0$, $\theta = 0.42°$, and $T = 35\,°$C.

IV. THE DEPENDENCE OF REFLECTION ON OTHER PARAMETERS

The competition between the absorption and the dispersion compensation can also be observed with the coupling fields detuned at $\theta = 0.42°$; see Fig. 5. In this case, the maximum reflection occurs at some detuning of the coupling field ($\Delta_c \neq 0$). When the coupling frequency is on-resonance ($\Delta_c = 0$) (see the black curve in Fig. 5), the reflection has a double peak because of the high absorption at two-photon resonance. When the coupling field is detuned, it is seen that the efficiency is even larger than that at the resonance because of the lower absorption at off-resonant coupling, and meanwhile, the phase-matching condition can still be satisfied with a corresponding detuning of the probe light (see the first term in Δk_x) so that higher efficiency can be obtained. On the other hand, the width of the reflection spectrum at resonant coupling is larger than that at the off-resonant coupling; it mainly results from two factors, the absorption and the dispersion compensation of phase mismatching.

The dependence of the reflection efficiency on the temperature of the vapor cell is shown in Fig. 6. Obviously, it is seen that the reflection efficiency increases with an increase in the temperature (i.e., an increase in the density of the atoms). The efficiency gets saturated at $T = 60\,°$C with reflection as high as 60%. In Fig. 7, it is shown that the reflection efficiency also strongly depends on the power of the coupling fields. We set the power of the co-propagating coupling field (P_{c1}) to equal that of the counterpropagating coupling field ($P_{c2} = P_{c1} = P_c$) where it reaches saturation at $P_c = 20$ mW for two different probe powers. On the contrary, 20% efficiency can still be obtained for a lower coupling power of 1 mW.

V. CONCLUSION

In this paper, we have experimentally and theoretically investigated the high-efficiency FWM in the Cs vapor EIT system under two counterpropagating coupling fields. The reflected intensity reaches more than 60% of the input probe

field with an input power of 300 μW. The high reflection is due to the two Doppler-free two-photon resonant processes, which result in the coherent reflection from all the atoms in the vapor cell in the reflection direction. The dependence of the reflection efficiency on the incident angle, the detuning and power of the coupling field, and the temperature of the vapor cell are also analyzed. Based on the discussion, we reach three related conclusions: As high as 60% efficiency reflection is obtained, which is explained with the enhanced FWM process in an EIT system; the two Doppler-free two-photon resonant processes are essential for efficient FWM; the complex mechanism of the dispersion compensation to phase mismatching and effective absorption length of a vapor cell induced by the absorption of the probe field also is investigated, which leads to an efficient reflection in a wide range of detunings and incident angles of the probe field. In the reflection direction, there is no original field and influence of Doppler background, and the detection sensitivity can be high, which may have potential applications in quantum-information processing and a quantum network proposed in atomic ensembles, such as the generation of nonclassical light for information processing, tunable optical switching, and so on.

ACKNOWLEDGMENTS

This work is supported by the National Basic Research Program of China (Nos. 2010CB923102 and 2011CB922203), the NSFC (Nos. 10974126 and 60821004), the RGC of the HK Government (No. HKBU202910), and the FRG of HKBU.

[1] S. L. Braunstein and P. van Loock, Rev. Mod. Phys. **77**, 513 (2005).
[2] S. E. Harris, Phys. Today **50**(7), 36 (1997).
[3] J. Gea-Banacloche, Y.-q. Li, S.-z. Jin, and M. Xiao, Phys. Rev. A **51**, 576 (1995).
[4] S. E. Harris, J. E. Field, and A. Imamoğlu, Phys. Rev. Lett. **64**, 1107 (1990).
[5] H. Schmidt and A. Imamoğlu, Opt. Lett. **21**, 1936 (1996).
[6] V. Boyer, C. F. McCormick, E. Arimondo, and P. D. Lett, Phys. Rev. Lett. **99**, 143601 (2007).
[7] V. Wong, R. S. Bennink, A. M. Marino, R. W. Boyd, C. R. Stroud Jr., and F. A. Narducci, Phys. Rev. A **70**, 053811 (2004).
[8] S. Du, E. Oh, J. Wen, and M. H. Rubin, Phys. Rev. A **76**, 013803 (2007).
[9] B. J. Feldman and M. S. Feld, Phys. Rev. A **5**, 899 (1972).
[10] S. A. Moiseev and B. S. Ham, Phys. Rev. A **73**, 033812 (2006).
[11] H. Kang, G. Hernandez, and Y. Zhu, Phys. Rev. A **70**, 061804 (2004).
[12] H. Y. Ling, Y.-Q. Li, and M. Xiao, Phys. Rev. A **57**, 1338 (1998).
[13] M. Bajcsy, A. S. Zibrov, and M. D. Lukin, Nature (London) **426**, 638 (2003).
[14] A. W. Brown and M. Xiao, Opt. Lett. **30**, 699 (2005).
[15] M. Artoni and G. C. La Rocca, Phys. Rev. Lett. **96**, 073905 (2006).
[16] A. Schilke, C. Zimmermann, P. W. Courteille, and W. Guerin, Phys. Rev. Lett. **106**, 223903 (2011).
[17] Y.-W. Lin, W.-T. Liao, T. Peters, H.-C. Chou, J.-S. Wang, H.-W. Cho, P.-C. Kuan, and I. A. Yu, Phys. Rev. Lett. **102**, 213601 (2009).
[18] Y. R. Shen, *The Principles of Nonlinear Optics* (Wiley, New York, 1984), p. 250.
[19] G. S. Agarwal and N. Nayak, Phys. Rev. A **33**, 391 (1986).
[20] B. R. Mollow, Phys. Rev. A **5**, 2217 (1972).
[21] G. C. Cardoso, V. R. de Carvalho, S. S. Vianna, and J. W. R. Tabosa, Phys. Rev. A **59**, 1408 (1999).
[22] S.-q. Kuang, R.-g. Wan, P. Du, Y. Jiang, and J.-y. Gao, Opt. Express **16**, 15455 (2008).
[23] J.-X. Zhang, H.-T. Zhou, D.-W. Wang, and S.-Y. Zhu, Phys. Rev. A **83**, 053841 (2011).
[24] Y. Dong, H. Wang, J. Gao, and J. Zhang, Phys. Rev. A **74**, 063810 (2006).
[25] D. Budker, W. Gawlik, D. F. Kimball, S. M. Rochester, V. V. Yashchuk, and A. Weis, Rev. Mod. Phys. **74**, 1153 (2002).
[26] S. I. Kanorsky, A. Weis, J. Wurster, and T. W. Hänsch, Phys. Rev. A **47**, 1220 (1993).
[27] P. F. Liao and G. C. Bjorklund, Phys. Rev. Lett. **36**, 584 (1976).
[28] F. Schuller and D. N. Stacey, Phys. Rev. A **60**, 973 (1999).
[29] A. K. Patnaik and G. S. Agarwal, Opt. Commun. **179**, 97 (2000).
[30] I. Novikova, A. B. Matsko, and G. R. Welch, Opt. Lett. **26**, 1016 (2001).
[31] R. L. Abrams and R. C. Lind, Opt. Lett. **2**, 94 (1978).